Numerical simulation of the generation of secondary electrons in the High Current Experiment

P. H. Stoltz*
Tech-X Corporation, 5541 Central Avenue, Suite 135, Boulder, Colorado 80301, USA

M. A. Furman and J.-L. Vay
Lawrence Berkeley National Laboratory, Berkeley, California 94720, USA

A. W. Molvik and R. H. Cohen
Lawrence Livermore National Laboratory, Livermore, California 94550, USA
(Received 4 April 2003; published 8 May 2003)

Electron effects in the High Current Experiment (HCX) are studied via computer simulation. An approximate expression for the secondary electron yield for a potassium ion striking stainless steel is derived and compared with experimental results. This approximate expression has a peak of roughly 55 electrons at normal incidence at an ion energy of 60 MeV. Using an empirical angular dependence, the secondary electron yield is combined with a numerical simulation of the HCX ion beam dynamics to obtain an estimate for the number of secondary electrons expected per ion-wall collision in the HCX. This estimate is that approximately 150–200 electrons per ion collision may result in the HCX.

DOI: 10.1103/PhysRevSTAB.6.054701 PACS numbers: 34.50.Dy, 52.20.Hv, 52.58.Hm, 79.20.Rf

I. INTRODUCTION

Electron effects presently limit the performance of many ion accelerators [1–3]. One source of these electrons is electrons emitted from collisions between beam ions and the beam pipe walls. Heavy-ion fusion (HIF) accelerators will operate with higher current than accelerators today [4], collisions between ions and the walls could be more frequent, and the accelerator costs are reduced if the wall is moved closer to the beam. Both effects increase the loss of beam ions to the wall, potentially increasing the production of electrons in an HIF power plant accelerator [5]. Consequently, designing HIF accelerators requires carefully studying electron effects. The goal of this paper is to discuss techniques used to estimate numerically the numbers of electrons researchers might expect in the heavy-ion fusion experiments, particularly the High Current Experiment [6] (HCX).

The HCX is the first transport experiment using a driver-scale heavy-ion beam. The experiment enables researchers to investigate topics such as beam size and quality during transport, measure the dynamic aperture of the HCX lattice, investigate how errors such as misalignments affect beam current, determine the extent of beam halo, and study secondary electron effects with driver-scale beam potentials (exceeding 1.0 keV). Such investigations were not possible with lower current HIF machines. The HCX uses a beam of singly charged potassium ions drifting through a six-quadrupole matching section and ten electrostatic transport quadrupoles. The HCX has a line-charge density (0.1–0.2 C/m), an injection energy (1–1.8 MeV), and a duration (4 μs) relevant to fusion drivers.

*Email address: pstoltz@txcorp.com

First, we derive an approximate expression for the secondary electron yield (SEY) for a potassium ion striking stainless steel. This approximation uses the results of Rothard *et al.* [7] to estimate the SEY in terms of the energy loss per unit length of potassium passing through stainless steel. We obtain an estimate of the energy loss per unit length from the SRIM [8] code. This gives an approximate SEY for potassium striking stainless steel with a peak of 55 electrons at an ion energy of roughly 60 MeV at normal incidence (this takes into account the inelastic part of the stopping power only). We implement a numerical model of this SEY curve by modifying the routines developed for the POSINST code [9]. This numerical model uses the energy at which the SEY peaks and includes an empirical fit to the dependence of the SEY on angle. We also compare the approximate SEY we derive here with data from the HCX and show the two agree well.

Next, we combine this SEY model with a particle dynamics model relevant to the HCX based on the WARP code [10]. The WARP simulation includes the full geometry of the HCX and self-consistent ion beam dynamics. From the WARP simulation, we determine the location, energy, and angle of the potassium ions striking the wall. Combining this with the SEY model gives an estimate of the number of electrons one can expect in the HCX. We estimate 150–200 electrons per ion-wall collision may occur in the HCX. However, we discuss how magnetic insulation could reduce the number of electrons reaching the beam center by an order of magnitude or more.

II. THEORY

In this section, we review the basic theory behind the model we use of secondary electron emission and the approximations we use to implement this model

numerically. First we discuss the relationship between SEY and energy loss per unit length. In particular, we discuss an expression by Rothard *et al.* for heavy-ion induced SEY and the numerical approximation of the SEY using the routines from the POSINST code. Second we discuss the dependence of SEY on the angle of incidence. We discuss the breakdown of the standard inverse cosine scaling and the measurements by Molvik of SEY as a function of angle for HCX. Finally, we use the data from HCX which do fit to inverse cosine scaling to extrapolate to normal incidence and compare with the approximate SEY developed here. The two agree within a percent.

The goal of this section is to develop an expression for the SEY for the ions and materials relevant to the HCX. The HCX uses potassium ions and stainless steel beam pipes. There is little experimental data for the SEY for potassium striking stainless steel as a function of energy, so we need a theoretical way to determine the SEY. One theoretical estimate of the SEY is based on the inelastic part of the energy loss per unit length [7]

$$\gamma_E = 0.14 C_b \frac{dE}{dx}, \tag{1}$$

where γ_E is the SEY, and dE/dx is the inelastic part of the energy loss per unit length in eV/Å. This equation applies strictly only when the inelastic stopping power is the dominant contribution to the ion stopping. The unitless $C_b \approx 0.32$ for heavy ions (values quoted by Rothard *et al.* for C_b range from 0.28 to 0.44, but have a mean of 0.32 for the ions and targets studied). The constant C_b represents the efficiency relative to protons for converting energy lost in a material to secondary electrons. By definition, $C_b = 1$ for protons. Potential reasons [11] C_b is less than 1 for heavier particles include (i) heavy ions may transfer more of their energy to target nuclei rather than target electrons (this fact can lead not only to a value of C_b less than 1, but a breakdown of the dependence of SEY on dE/dx as discussed below), (ii) heavy ions may create larger ion channels in their wake, which can trap secondary electrons, and (iii) a breakdown of first-order ionization theories [12].

The relationship in Eq. (1) between secondary electron yield and energy loss per unit length will break down if a significant fraction of secondary electrons comes from a source other than from the inelastic stopping of the heavy ion. For instance, target ions recoiling from an elastic collision with the incident heavy ion could themselves produce secondary electrons. An estimate [11] of the maximum ratio of secondary electrons due to recoiling target ions is

$$\frac{\gamma_{\text{recoil}}}{\gamma_E} = \frac{2}{3}\left(\frac{Z_t}{Z_p}\right)^{1/6}\left(\frac{Z}{Z_t}\right)^{2/3}\left(\frac{M_p}{M_p + M_t}\right)^2, \tag{2}$$

where M_p and M_t are the mass of the projectile and target, Z_p and Z_t are the atomic numbers of the projectile and target, and $Z^{2/3} = Z_p^{2/3} + Z_t^{2/3}$. This approximation applies in the energy range of the maximum of the elastic stopping power. For the HCX, we consider potassium projectiles incident on a stainless steel target. The stainless steel target is 70% iron, so for this estimate we use the $M_t = M_{\text{Fe}}$ and $Z_t = Z_{\text{Fe}}$. In this case, Eq. (2) estimates at maximum this ratio is 22%. This estimate agrees to within a few percent with results of SRIM, which predicts for 1.0 MeV potassium in stainless steel, the energy lost to target electrons is 206.4 eV/Å, and the energy lost to target ions is 44.7 eV/Å, yielding a ratio of 21.7%. We consider this small enough to neglect for this work. We also neglect effects such as electrons produced by one-electron plasmon decay [11].

For the expression in Eq. (1), we need to know the inelastic energy loss rate, dE/dx, for potassium in stainless steel. We can estimate the inelastic part of dE/dx for a potassium ion stopping in stainless steel using the SRIM code [8]. The SRIM code uses a quantum mechanical treatment of the ion-target collisions to calculate the stopping of ions in matter. SRIM includes effects such as a screened Coulomb collision with exchange and correlation interactions between the overlapping electron shells, and long range interactions creating electron plasmons in the target. The ion charge state is described using *effective charge*, and includes a velocity-dependent charge state and long range screening due to the electrons in the target material. The SRIM result we use is a stopping cross section for potassium averaged over many target materials. The energy loss per unit length, dE/dx, is related to the stopping cross section by

$$\frac{dE}{dx} = S_\sigma \rho, \tag{3}$$

where S_σ is the stopping cross section in units of energy area and ρ is the number density of the target material. In the HCX, the stainless steel has a mass density of approximately 8.03 g/cm^{-3} and a composition of roughly 70% Fe, 20% Cr, and 10% Ni, giving a number density of approximately $\rho = 8.63 \times 10^{22}$ cm^{-3}. The SRIM result for the inelastic part of dE/dx for a potassium ion stopping in stainless steel, converted using Eq. (3), is shown in Fig. 1. Using this result for the inelastic stopping in Eq. (1) with $C_b = 0.32$ gives an approximate SEY for potassium ions incident on stainless steel. This SEY curve is shown in Fig. 2 as the solid line. This approximation takes into account only the inelastic part of the stopping, but as we showed with the help of Eq. (2), the elastic contributions will be small even in the worst case.

To implement a numerical model of the estimated SEY, we use routines from the POSINST code [9]. Researchers have used the POSINST code to study electron effects in the Los Alamos Proton Storage Ring [1], the Argonne Advanced Photon Source [13], the Spallation Neutron Source [14], and the CERN Large Hadron Collider [15]. The POSINST routines approximate the true secondary

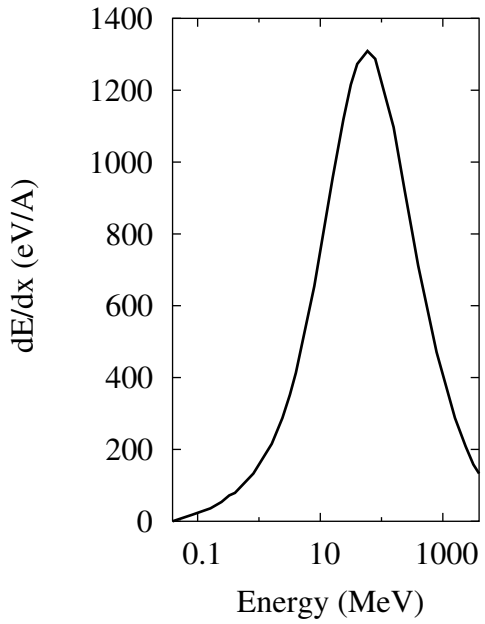

FIG. 1. Estimated inelastic energy loss per unit length (eV/Å) for potassium in stainless steel as a function of the potassium ion energy. This is derived from Eq. (3) using a number density for stainless steel of $\rho = 8.63 \times 10^{22}$ cm^{-3} and the results of the SRIM code for the stopping cross section of potassium in an arbitrary target material.

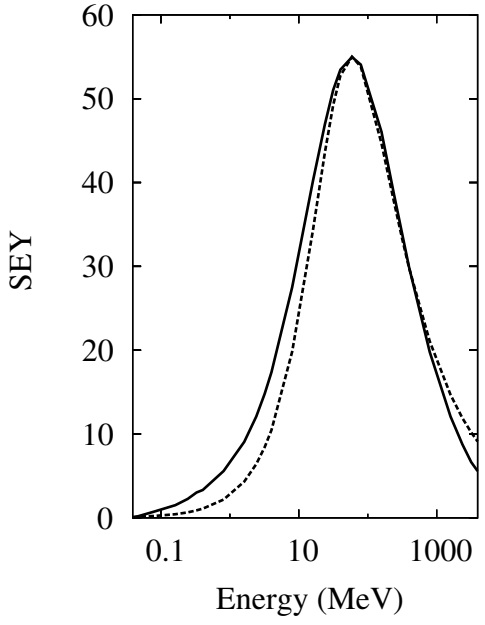

FIG. 2. The estimated secondary electron yield (SEY) for potassium ions impacting on stainless steel as a function of the incident ion energy at normal incidence, shown as the solid line. The estimated SEY is from Eq. (1) with $C_b = 0.32$ and the inelastic energy loss per unit length from Fig. 1. A numerical fit from Eq. (4) with $s = 1.53$ is shown as the dashed line.

component of the SEY by the formula

$$\frac{\gamma}{\gamma_{\max}} = \frac{sx}{s - 1 + x^s}, \tag{4}$$

where x is the incident energy of the ion, scaled to the value at which the SEY curve peaks (approximately 60 MeV in this case), and s is a unitless fitting parameter. Over the entire range of energies shown in Fig. 2, the best fit using Eq. (4) is for $s = 1.53$. This fit is shown as the dashed line in Fig. 2. However, for the application to the HCX, we are interested in energies near the few MeV range, and so we choose a value of $s = 1.23$, which better fits the low energy end, as shown in Fig. 3.

Next, we need a model of the dependence of the SEY on the incident angle of the ion. The SEY curve shown in Fig. 2 is for normal incidence. However, ions in the HCX will not strike the walls at normal incidence, but rather will graze against the walls. The conventional model for the dependence of SEY on angle is

$$\gamma = \frac{\gamma_0}{\cos\theta}, \tag{5}$$

where γ_0 is the SEY at normal incidence, and θ is the angle relative to normal. This model is based on the argument that the secondary electrons are emitted from within a distance d of the surface, and the amount of the incident particle's path that lies within a distance d of the surface increases as $1/\cos\theta$. The distance d is called the *escape zone* and is typically on the order of a few nanometers [16]. The model in Eq. (5) eventually breaks down at a large enough angle. Some reasons for the breakdown are that as the path length within the escape zone gets larger (i) the ion would deposit all its energy and come to rest, (ii) the ion will have more chances to undergo scattering events which could knock it out of the escape zone (this is discussed further below), and (iii) ions incident at highly grazing angles may not penetrate the surface at all and instead may just skip off the surface. For various heavy ions incident on stainless steel, Thieberger *et al.* [17] at Brookhaven National Laboratory have measured nearly inverse cosine behavior to beyond 89° for smooth surfaces [Thieberger *et al.* fit the data to $(\cos\theta)^{-f}$, with $f = 0.96 - 1.152$ for different ions]. For 1.0 MeV potassium ions on stainless steel at the HCX, Molvik has measured inverse cosine behavior to approximately 86°. Molvik's results are shown in Fig. 4. For our numerical model of the angular dependence of the SEY in the HCX, we use a cubic spline fit to the data in Fig. 4 with a linear extrapolation past 88°.

One can use the large-angle data of Molvik to provide a check on the estimated SEY developed here. Because the measurements of Molvik fit well to inverse cosine scaling below 86°, one can assume such scaling to project the SEY back to normal incidence and compare that value for SEY with the estimated SEY for 1.0 MeV from Fig. 2. At 80°, Molvik measured an SEY of roughly 36. Plugging these values into Eq. (5) and solving for γ_0 yields $\gamma_0 \approx 6.0$ (using other data points between 80° and 86° gives the

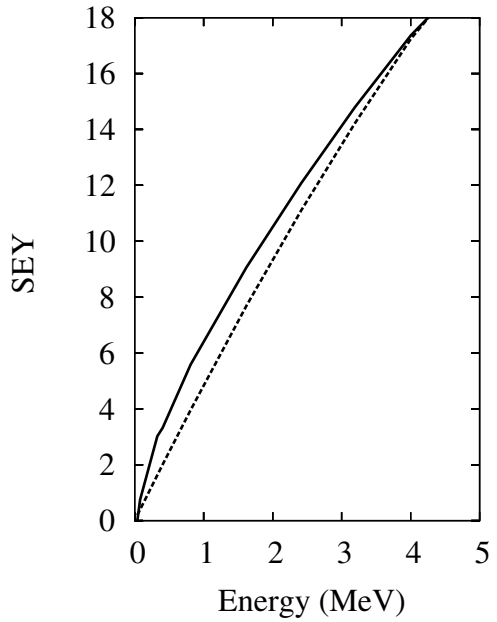

FIG. 3. A fit to the SEY for the low-energy range 0–5 MeV. The solid line is the estimated SEY as discussed in Fig. 2. A numerical fit from Eq. (4) with $s = 1.23$ is shown as the dashed line. This low-energy range is the range of interest for modeling the HCX.

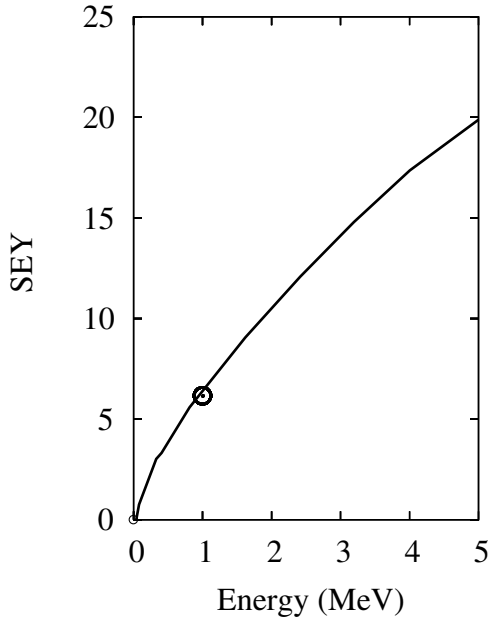

FIG. 5. A comparison of the estimated SEY for potassium incident on stainless steel and data taken at the HCX. The solid line is the estimate SEY as discussed in Fig. 2. The circle is a based on extrapolating the data from the HCX in Fig. 4 to normal incidence. The agreement between the estimated SEY and the HCX data for 1.0 MeV gives confidence in the estimated SEY.

same result for γ_0 to less than a percent). This is shown as the circle in Fig. 5, with the estimated SEY from Fig. 2 shown as the solid line. While only for a single energy, the agreement between the estimated SEY and the HCX data point gives us added confidence in the validity of the estimated SEY.

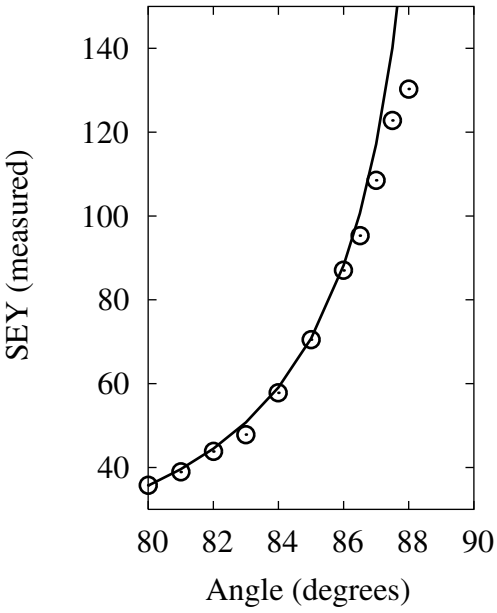

FIG. 4. The measured secondary electron yield as a function of incident angle for 1.0 MeV potassium ions striking stainless steel as measured at the HCX. The measured values are shown as circles. The solid line is a fit to $1/\cos\theta$. The measured values begin to deviate from inverse cosine scaling past 86°.

III. RESULTS FOR THE HCX

In this section, we apply our numerical models of the SEY to a simulation relevant to the HCX. We use the results of a detailed particle-in-cell simulation of an HCX-like geometry to estimate the likely location, energy, and angle with which ions might strike the wall in the HCX. Using this information and the numerical models developed above, we estimate 150–200 electrons per ion collision could result in the HCX.

To estimate the number of secondary electrons in the HCX, we need to know the energy and angle at which stray ions might likely strike the walls. This information comes from a detailed particle tracking simulation relevant to HCX using the WARP code [10] (this simulation used a higher filling factor for the focusing elements than the present HCX configuration, but the parameters are still realistic). WARP is a multidimensional particle-in-cell code with many advanced features, such as fully 3D applied fields and multigrid field solvers. We used results of a simulation of a 20 m long electrostatic quadrupole transport segment with 100 quadrupoles and a 2.3 cm radius beam pipe.

The WARP results show that for the parameters chosen, all the ions strike the wall with a kinetic energy of $E_k =$

1.85 MeV (to within a few percent). Figure 6 shows a scatter plot of the angle of incidence of these particles as a function of their distance down the 20 m transport section. The angles of incidence range from about 84° to 89.97°. There are fewer particles at larger z because ions are being scraped off and therefore fewer ions are striking the walls at larger z. In the simulation, the beam was perfectly matched to the lattice.

Using these results for energy and angle, we can apply our numerical model for secondary electron yield to estimate the electrons one can expect in the HCX. Figure 7 shows the number of electrons per ion collision as a function of distance generated by combining the stray ion data from WARP with the SEY model discussed above. This figure shows a yield of roughly 150 electrons per ion collision near $z = 0$, with a general increase to approximately 180–185 with increasing z. The increase with distance is due to the increasing SEY as a function of incident angle and the fact that the average angle of incidence increases with increasing z, as one can see in Fig. 6. Past $z \approx 5.0$ m, we expect this result is an upper limit and is accurate only to approximately 10%, due to the extrapolation of the angular dependence of the SEY past 88°. The estimate of 10% accuracy comes from the difference in SEY if the SEY as a function of angle leveled off rather than continued to increase linearly past 88° (Thieberger *et al.* [17] observed for gold ions that the SEY not only leveled off but began to decrease with increasing angle, in which case the error could be slightly larger than 10%).

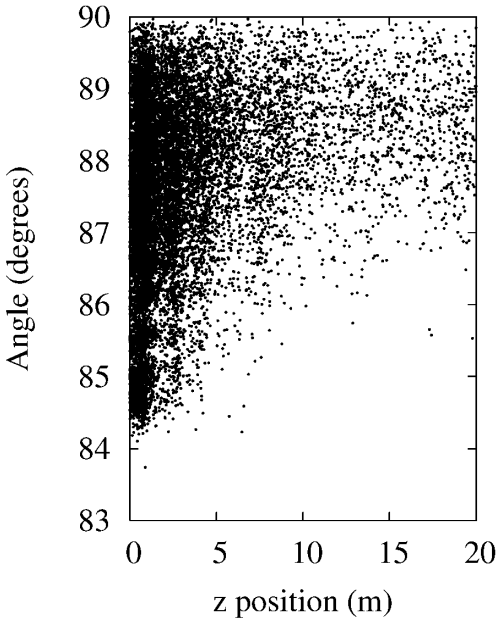

FIG. 6. The angle of incidence versus distance for ions striking the wall in a WARP simulation of potassium ions in a 20 m electrostatic quadrupole transport section, relevant to the HCX.

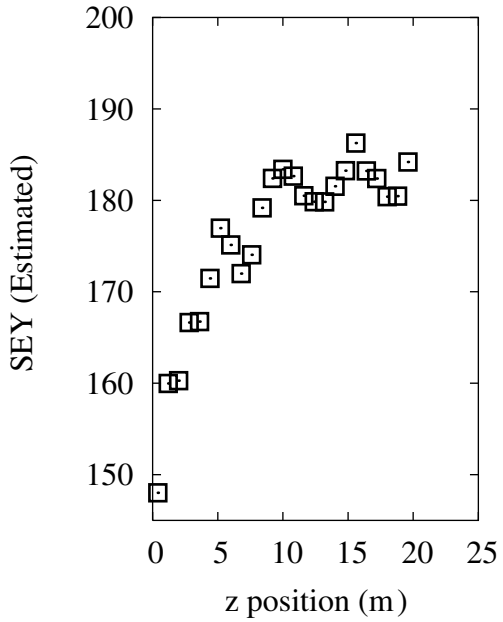

FIG. 7. Estimated number of electrons per ion collision as a function of distance in the HCX-relevant system modeled by WARP. The increase with distance is due to the particles at larger z striking the wall with larger angle, as shown in Fig. 6, which results in a larger SEY.

IV. CONCLUSION

We have modeled numerically secondary electron generation in the High Current Experiment. We derived an approximate expression for the secondary electron yield for potassium ion striking stainless steel and showed the approximate SEY agreed well with data from the HCX. This estimate has a peak of approximately 55 electrons at normal incidence at an ion energy of 60 MeV. To estimate the electron yield in HCX, we combined that expression and an empirical model of the angular dependence with a particle-in-cell simulation relevant to HCX ion beam dynamics. This estimate is that approximately 150–200 electrons per ion collision may result in the HCX.

This work is merely a starting point in studying electron effects in heavy-ion fusion devices, as we have neglected many important effects. These include surface roughness [17] and effects of the secondary electrons on the ion beam dynamics, among others. We also neglect ion skimming. From Fig. 6, one can see many particles with an angle of incidence between 89° and 90°. These particles are likely to skim along the surface, producing secondary electrons in a manner much different than considered here. Further, we have neglected the production of neutral gas atoms from the ion-wall collisions. The neutrals could drift to the beam where they might be ionized by collisional impact, resulting in another source of electrons within the beam.

A further effect we have neglected and that deserves specific mention is the effect of magnetic fields on

secondary electron motion. Researchers expect a fraction 10^{-3} of the beam particles could strike the wall in an accelerator for HIF. Having 150–200 electrons per collision in that case could mean an electron charge density that is approximately 15%–20% of the ion charge density. Other researchers have suggested even a 10% electron charge density can severely disrupt the ion beam via the two-stream instability [18]. However, the two-stream instability is based on the assumption that the electrons and ions overlap. The electrons produced by ion-wall collisions are generated at the wall, and so one can mitigate their effect if one can keep them from reaching the beam. One way to accomplish this is to constrain the electrons with a magnetic field to keep them from crossing the vacuum gap to the beam, a process called *magnetic insulation* [19]. Because secondary electrons are born with energies much lower than the ion beam, one can use even low-level magnetic fields to constrain the electrons and not affect the ion motion. Quadrupole fields are particularly interesting because (i) an actual accelerator will likely be using magnetic quadrupoles for beam focusing anyway, and (ii) the beam is most elliptical in a quadrupole and therefore increasing likely to collide with the wall. Research into the effects of quadrupole magnetic fields on secondary electron orbits [20–22] suggests quadrupole fields can reduce by many orders of magnitude the number of secondary electrons near the beam center as compared to field-free cases (see, for instance, Fig. 18 of Ref. [20]). Researchers in pulsed power physics rely on magnetic insulation in a similar way to contain stray electrons in high-power waveguides [23].

ACKNOWLEDGMENTS

The authors thank A. Friedman, C. Celata, and D. Grote for many suggestions regarding this work. This work was funded by the Department of Energy, in part by the Office of Fusion Energy Science through the SBIR program, in part under Contract No. DE-AC03-765F00098, and in part under the auspices of the U.S. Department of Energy by the University of California at Lawrence Livermore National Laboratory under Contract No. W-7405-ENG_48.

[1] M. Blaskiewicz, M. A. Furman, M. Pivi, and R. J. Macek, Phys. Rev. ST Accel. Beams **6**, 014203 (2003).

[2] W. Fischer, J. M. Brennan, M. Blaskiewicz, and T. Satogata, Phys. Rev. ST Accel. Beams **5**, 124401 (2002).

[3] K. Ohmi, T. Toyama, and C. Ohmori, Phys. Rev. ST Accel. Beams **5**, 114402 (2002).

[4] *Proceedings of the 12th International Symposium on Heavy Ion Inertial Fusion*, edited by I. Hofmann [Nucl. Instrum. Methods Phys. Res., Sect. A **415**, 1–725 (1998)].

[5] A. Molvik, in Proceedings of the 14th International Symposium on Heavy Ion Inertial Fusion, Moscow, 2002 [Laser Part. Beams (to be published)].

[6] P. A. Seidl, in Proceedings of the 14th International Symposium on Heavy Ion Inertial Fusion, Moscow, 2002 (Ref. [5]).

[7] H. Rothard, K. Kroneberg, A. Clouvas, E. Veje, P. Lorenzen, N. Keller, J. Kemmler, W. Meckbach, and K.-O. Groeneveld, Phys. Rev. A **41**, 2521 (1990).

[8] J. F. Ziegler, J. P. Biersack, and U. Littmark, *The Stopping and Range of Ions in Solids* (Pergamon Press, New York, 1985).

[9] M. A. Furman and M. Pivi, Phys. Rev. ST Accel. Beams **5**, 124404 (2002).

[10] A. Friedman, Part. Accel. **37–38**, 131 (1992).

[11] D. Hasselkamp, in *Particle Induced Electron Emission II*, edited by G. Hohler (Springer-Verlag, New York, 1992).

[12] M. Beuve, M. Caron, P. Fainstein, M. Galassi, M. Gervais, R. D. Rivarola, and H. Rothard, Eur. Phys. J. D **21**, 125 (2002).

[13] M. A. Furman, M. Pivi, K. C. Harkay, and R. A. Rosenberg, in *Proceedings of the Particle Accelerator Conference, Chicago, 2001* (IEEE, Piscataway, NJ, 2001), p. 679.

[14] M. T. F. Pivi and M. A. Furman, Phys. Rev. ST Accel. Beams **6**, 034201 (2003).

[15] M. A. Furman and M. Pivi, in *Proceedings of the Particle Accelerator Conference, Chicago, 2001* (Ref. [13]), p. 1898.

[16] H. Seiler, Z. Angew. Phys. **22**, 249 (1967).

[17] P. Thieberger, A. L. Hanson, D. B. Steski, V. Zajic, S. Y. Zhang, and H. Ludewig, Phys. Rev. A **61**, 042901 (2000).

[18] H. Qin, E. A. Startsev, and R. C. Davidson, Phys. Rev. ST Accel. Beams **6**, 014401 (2003).

[19] R. C. Davidson, *Physics of Nonneutral Plasmas* (Addison-Wesley, Boston, MA, 1990).

[20] L. F. Wang, H. Fukuma, K. Ohmi, S. Kurakowa, and K. Oide, Phys. Rev. ST Accel. Beams **5**, 124402 (2002).

[21] R. Cohen, A.W. Molvik, and J. L. Vay, Bull. Am. Phys. Soc. **47**, RP1.063 (2002).

[22] P. Stoltz, Bull. Am. Phys. Soc. **47**, RP1.061 (2002).

[23] O. Boine-Frankenheim, T. Pointon, and T. Mehlhorn, Nucl. Instrum. Methods Phys. Res., Sect. A **415**, 473 (1998).